116 *Biochemistry* **2011,** *50,* 116–124
DOI: 10.1021/bi101316y

BIOCHEMISTRY
including biophysical chemistry & molecular biology
Article

Multiple, Distributed Interactions of μ-Conotoxin PIIIA Associated with Broad Targeting among Voltage-Gated Sodium Channels†

Jeff R. McArthur,‡ Vitaly Ostroumov,‡ Ahmed Al-Sabi,‡ Denis McMaster,§ and Robert J. French*,‡

‡*Department of Physiology and Pharmacology, Faculty of Medicine, and Hotchkiss Brain Institute and* §*Department of Biochemistry and Molecular Biology, Faculty of Medicine, University of Calgary, Calgary, Alberta T2N 4N1, Canada*

Received August 16, 2010; Revised Manuscript Received November 18, 2010

ABSTRACT: The first μ-conotoxin studied, μCTX GIIIA, preferentially blocked voltage-gated skeletal muscle sodium channels, $Na_v1.4$, while μCTX PIIIA was the first to show significant blocking action against neuronal voltage-gated sodium channels. PIIIA shares >60% sequence identity with the well-studied GIIIA, and both toxins preferentially block the skeletal muscle sodium channel isoform. Two important features of blocking by wild-type GIIIA are the toxin's high binding affinity and the completeness of block of a single channel by a bound toxin molecule. With GIIIA, neutral replacement of the critical residue, Arg-13, allows a residual single-channel current (~30% of the unblocked, unitary amplitude) when the mutant toxin is bound to the channel and reduces the binding affinity of the toxin for $Na_v1.4$ (~100-fold) [Becker, S., et al. (1992) *Biochemistry 31*, 8229−8238]. The homologous residue in PIIIA, Arg-14, is also essential for completeness of block but less important in the toxin's binding affinity (~55% residual current and ~11-fold decrease in affinity when substituted with alanine or glutamine). The weakened dominance of this key arginine in PIIIA is also seen in the fact that there is not just one (R13 in GIIIA) but three basic residues (R12, R14, and K17) for which individual neutral replacement enables a substantial residual current through the bound channel. We suggest that, despite a high degree of sequence conservation between GIIIA and PIIIA, the weaker dependence of PIIIA's action on its key arginine and the presence of a nonconserved histidine near the C-terminus may contribute to the greater promiscuity of its interactions with different sodium channel isoforms.

Voltage-gated sodium (Na_v)[1] channels power the fast rising phase of action potentials, thus driving a self-propagating electrical signal along the surface membrane of excitable cells (*1*). Inward current through Na_v channels underlies electrical signaling in tissues, including central and peripheral nerves, skeletal muscle, and heart. Members of the Na_v channel family are classified as $Na_v1.1$−1.9 according to their α-subunit sequence (*2*). Mutations in different sodium channel subtypes lead to various maladies, including, myotonias, cardiac arrhythmias, epilepsies, and pain (*3*). Identification of the molecular determinants of Na_v isoform-specific block by different μ-conotoxins (μCTXs) could stimulate development of targeted drugs for combatting hyperexcitability disorders in particular tissues (*4*).

The first μCTX peptides were isolated from the venom of cone snails more than three decades ago (*5*−*7*). To date, all μCTXs isolated have come from fish-hunting cone snails, whose venoms rapidly induce paralysis following injection into the prey fish. Three different *Conus* peptide families are known to target Na_v channels, and all three are found together in the venoms of various cone snails. The μCTXs, including GIIIA and PIIIA, are channel blockers, while the δCTXs, including PVIA, delay or inhibit fast inactivation of the channel. Finally, the μO-CTXs, so far found only in the venom of *Conus marmoreus* (*8*), inhibit sodium conductance, but unlike the μCTXs, these do not appear to act by directly blocking the pore.

μCTXs GIIIA−C were first obtained from the fish hunter *Conus geographus* (*5*, *7*), but other μCTXs have since been isolated from various *Conus* species, including *Conus stercusmuscarum* [SmIIIA (*9*)], *Conus striatus* [SIIIA (*10*)], *Conus consors* [CnIIIA/B (*11*)], *Conus catus* [CIIIA (*11*)], *Conus magus* [MIIIA (*11*)], *Conus kinoshitai* [KIIIA (*10*)], *Conus tulipa* [TIIIA (*12*)], and *Conus purpurascens* [PIIIA (*13*)]. μCTXs are disulfide-rich peptides ranging from 16 to 25 amino acids in length. μCTXs interact with site 1, in the pore outer vestibule, and appear to block current flow by a combination of steric occlusion and electrostatic repulsion (see ref *14* for a recent review). The isoform specificity varies among the different μCTXs, providing peptide probes for studying the pore regions of various sodium channel isoforms.

The venom from *C. purpurascens* has provided conopeptides, including μCTX PIIIA and δCTX PVIA (*15*), that target voltage-gated sodium channels and κCTX PVIIA, targeting voltage-gated potassium channels (*16*). In this work, we focus on some functional properties of μCTX PIIIA. The μCTX PIIIA sequence was determined from mRNA isolated from the venom ducts of

†R.J.F. was supported as an AHFMR Medical Scientist and by operating grants from CIHR (MOP-10053) and from HSF of Alberta, Northwest Territories, and Nunavut. J.R.M. holds an AHFMR studentship.

*To whom correspondence should be addressed: Department of Physiology and Pharmacology, University of Calgary, 3330 Hospital Dr. NW, Calgary, AB T2N 4N1, Canada. Telephone: (403) 220-6893. Fax: (403) 210-7446. E-mail: french@ucalgary.ca.

[1]Abbreviations: CTX, conotoxin; BTX, batrachotoxin; GFP, green fluorescent protein; Na_v, voltage-gated sodium; rSkM1, rat skeletal muscle Na_v channel; HEK 293 cell line, human embryonic kidney; K_d, apparent dissociation constant; k_{on}, association rate constant; k_{off}, dissociation rate constant; F_{res}, fractional residual current; IC_{50}, steady-state half-blocking concentration; P_o, channel open probability; P_{tx}, toxin bound probability.

 Published on Web 11/29/2010

C. purpurascens (*13*). μCTX PIIIA is a 22-amino acid peptide, containing atypical amino acids pyroglutamate and hydroxyproline, as well as an amidated C-terminus. The solution structure of μCTX PIIIA was determined by NMR spectroscopy, and the toxin was further studied by radioligand binding and structure calculations (*17*). Despite the high degree of sequence similarity and the same disulfide bond pattern that is found in μCTX GIIIA, μCTX PIIIA shows a significant binding affinity for neuronal Na_v channels, while still being a more potent blocker of skeletal muscle Na_v channels (*18*).

Here, we examine the interaction of μCTX PIIIA with Na_v channel isoforms from skeletal muscle ($Na_v1.4$) and nerve ($Na_v1.2$). We used single substitutions, and a triple amino acid replacement of specific residues in the toxin, to investigate how individual amino acids affect toxin binding, single-channel conductance, and toxin selectivity among different sodium channel isoforms. Replacements were chosen either to replace important basic residues or to mimic more closely the μCTX GIIIA sequence. Our results indicate that for the less selective toxin, PIIIA, there is a broader distribution on the toxin's surface of residues that are important for high affinity or critical for the complete block of a single-channel current.

EXPERIMENTAL PROCEDURES

Rat Skeletal Muscle Preparation. Membrane vesicles were isolated from adult rat skeletal muscle as described previously (*19*). Briefly, the skeletal muscle from one or two adult rats was used to isolate rat skeletal muscle sodium channels (rSkM1). The muscle was homogenized in an isotonic sucrose solution with a food processor and then centrifuged for 10 min at 5000*g*. The supernatant was then filtered through six layers of cheese cloth. The pellet was resuspended in an isotonic sucrose solution (100 mg/mL sucrose, 2 mg/mL sodium azide, and 10 mM MOPS, adjusted to pH 7.4 with NaOH or HCl via addition of 34.8 mg/L phenylmethanesulfonyl fluoride at beginning of the protocol), and the mixture was homogenized and then spun again at 5000*g* for 10 min. The supernatant was filtered through the cheese cloth to remove the material that did not homogenize and combined with the supernatant from the previous step. KCl was added to the supernatant (final concentration of 0.6 M) to solubilize the muscle contractile elements, and then the mixture was spun at 8000*g*. The supernatant was passed through cheese cloth, collected, and spun for 40 min at 160000*g*. The resulting pellet was resuspended in ~100 mL of isotonic sucrose buffer, homogenized with a glass−Teflon homogenizer, and then spun for 10 min at 10500*g*. The supernatant was collected and spun for 40 min at 150000*g*. The resulting pellet was resuspended in ~15 mL of isotonic sucrose buffer, homogenized again with a glass−Teflon homogenizer, and layered on top of a sucrose gradient (35 to 25% sucrose with 10 mM MOPS). The gradient was then spun overnight (12−18 h) at 90000*g*.

The next day, the band at the interface was removed and divided into two 26 mL tubes, filled with cold distilled water, and spun for 50 min at 100000*g*. The resulting pellet was then resuspended in 0.3 M sucrose and 20 mM HEPES to a protein concentration of ~1.5 mg/mL (Bradford assay).

Toxin Synthesis and Preparation. Conotoxin synthesis, purification, and disulfide bond formation were performed by D. McMaster (Peptide Services, Faculty of Medicine, University of Calgary), as previously described (*20*). Briefly, solid-phase synthesis using 9-fluorenylmethoxycarbonyl (Fmoc) chemistry was used to synthesize linear peptides. Coupling of Fmoc amino acids was performed on an Applied Biosystems 431A synthesizer utilizing the HBTU/HOBT/DIPEA method. The linear peptide purified by high-performance liquid chromatography (HPLC) was subjected to oxidative folding under equilibrium conditions, by air oxidation in the presence of a small amount of mercaptoethanol (10 μL in 150 mL), to promote formation of the most stable disulfide bonds. Folding of the peptide during the oxidation was monitored by analytical HPLC over the course of 2−4 days at 4 °C. The peptides formed a single major peak with a few smaller minor peaks seen in each case depending on the derivative being cyclized. The crude peptide was isolated from the acidified reaction mixture by reverse-phase extraction and purified to near homogeneity by HPLC, and the identity was confirmed by quantitative amino acid analysis and by MALDI mass spectrometry molecular weight determination.

Conotoxin peptide derivatives were dissolved in doubly distilled, deionized water at a stock concentration of 100 μM. The stock solution was further diluted using a recording solution to the required concentration for individual experiments.

Single-Channel Recordings from Planar Lipid Bilayers. The rSkM1 preparation (tissue preparation predominantly contains $rNa_v1.4$) was taken from the freezer (−80 °C) and incubated on ice with batrachotoxin (BTX, 1 μM) for a minimum of 1 h before it was used for incorporation of the channel into the bilayer. For this incubation, an aliquot of BTX stock (1 μM in ethanol) was evaporated in a stream of nitrogen immediately before use. In the experiments, we used a horizontal chamber (P. Byrne, Biomedical Technical Support Centre) with two compartments, each ~200 μL, to hold the "extracellular" and "intracellular" solutions [200 mM NaCl, 10 mM HEPES, and 0.1 mM EDTA (pH 7.0)]. Symmetrical solutions were used for all experiments. The two compartments were separated by a plastic partition (photocopy transparency film) (*21*), penetrated using a small sewing needle, or the beam of a femtosecond laser (Y. Tu, Department of Mechanical and Manufacturing Engineering, University of Calgary), with a small hole ~60−100 μm in diameter, across which the bilayer was formed. The bilayers were painted with a mixture of phosphatidylethanolamine (PE) and phosphatidylcholine (PC) (40 and 10 mg/mL, respectively, in decane) across the partition. Prior to bilayer formation, the current offset, at the output of the patch clamp amplifier, using symmetric chamber solutions, was balanced to zero, to define a transmembrane holding voltage (V_m) of 0 mV.

Upon formation of a bilayer, 1 μL of the rSkM-1 in BTX was pipetted over the bilayer and incorporation was detected at ±60 mV as a step increase in current amplitude of ~1 pA. Once incorporation was seen, the orientation of the channel in the bilayer was determined by checking for voltage-dependent gating at ±70 mV. The toxin was then perfused to the extracellular side of the channel (2 × 400 μL) and recorded at ±40 mV to record single-channel blocking event kinetics. Records lasted 51.0 ± 3.8 (66) min, allowing many distinct toxin blocking events to be recorded at both voltages. All measurements were taken with an Axopatch 200 (Molecular Devices Corp., Sunnyvale, CA) integrating patch amplifier (low-pass filtered with a corner frequency of 1kHz; Bessel, 80 dB/decade), filtered again with a low-pass filter at 100 Hz, and digitized (sampling frequency of 200 Hz) with a Digidata 1322A 16-bit acquisition system (Molecular Devices Corp.). The records were monitored on a digital oscilloscope (model 2090-IIIA, Nicolet Instrument Corp.) and recorded both digitally with pClamp 9.2 (Molecular Devices Corp.) and at

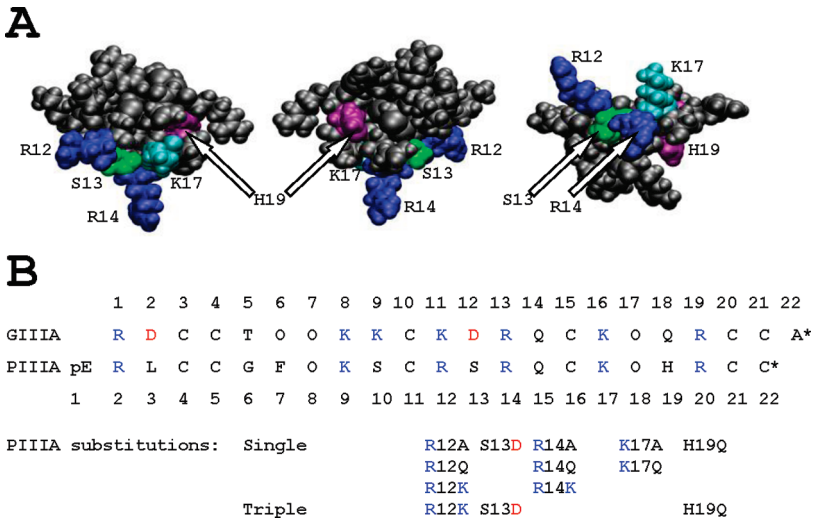

FIGURE 1: Space-filling (van der Waals) representation of PIIIA and sequence alignments of μCTX GIIIA and μCTX PIIIA. (A) van der Waals structure of μCTX PIIIA created in VMD (*36*) using coordinates from Protein Data Bank (*37*) entry 1R9I, from three perspectives showing important residues mapped onto the surface of the toxin. (B) Sequence alignment of μCTX PIIIA and GIIIA based on alignment of their disulfide bonds, with all 10 single substitutions, and the triple mutant used in the paper shown below. Basic residues (blue or turquoise) and acidic residues (red) are highlighted. pE, pyroglutamate; O, hydroxyproline. An asterisk denotes C-terminal amidation.

low speed (~1 mm/s) on chart paper (General Scanning Inc., model RS2-5P).

Whole-Cell Patch Clamp Recordings. Macroscopic currents were recorded using the whole-cell patch clamp technique (*22*) at room temperature (22−24 °C). HEK 293 cells were transiently cotransfected with either an $Na_v1.2$ in pCDM8, a gift from W. A. Catterall (*23*), or $Na_v1.4$ clone (*24*) in pCDNA3.1 (Invitrogen Corp., Carlsbad, CA) and a plasmid encoding GFP, allowing transfected cells to be identified by their green fluorescence. Pipette electrodes had final tip resistances of 1−3 MΩ. The bath solution contained 140 mM NaCl, 5 mM KCl, 2 mM $CaCl_2$, 1 mM $MgCl_2$, 10 mM HEPES, and 10 mM glucose, with the pH adjusted to 7.4 with NaOH. Selected concentrations of toxin were added to the bath solution. The pipette solution contained 35 mM NaCl, 105 mM CsF, 1 mM $MgCl_2$, 10 mM HEPES, and 1 mM EGTA, with the pH adjusted to 7.2 with CsOH.

Voltage clamp was conducted with a patch amplifier (EPC7, HEKA Electronics Inc., or an Axopatch 200B, Axon Instruments, Inc.). Current traces were filtered at 3 kHz (low-pass, three-pole Bessel filter, EPC7) and sampled at 200 kHz using pClamp version 9.2 (Axon Instruments, Inc.). Only cells expressing peak sodium currents between 1 and 5 nA were used, to ensure good current resolution while maintaining adequate voltage control. Series resistance was typically compensated at 50−60%. Continuous local superfusion of the toxin was maintained during experimental recordings with the flow rate maintained at 10−20 μL/min (bath volume of 5 mL). Washout began only after the peak currents had reached a steady-state level. Equilibrium half-blocking concentrations (IC_{50}) and kinetics of μCTX PIIIA and the corresponding derivatives were calculated from records using a holding potential of −80 mV, with a 2 s prepulse to −140 mV followed by a test pulse to −10 mV. This pulse sequence was repeated every 5 s, in the presence and absence of the toxin, and during washout.

Data Analysis. Single-channel data were analyzed by determining the probability of the channel being in the open (P_o) and toxin-bound (P_{tx}) states using Clampfit version 9.2 (Molecular Devices Corp.). All steady-state bilayer records were filtered digitally after the completion of the experiment using a low-pass Gaussian filter at 20 Hz over the entire trace. A single-channel search using a half-amplitude detection threshold was performed to identify the probabilities of the open and toxin-bound periods. From the probabilities, we calculated the apparent dissociation constant (K_d) using the equation $K_d = [Tx](P_o/P_{tx})$. For each toxin derivative, K_d values were calculated at ±40 mV ($n \geq 3$ at each voltage for each toxin derivative). The K_d values were plotted against potential difference (V) and fit using the equation $K_d(V) = K_d(0\text{ mV}) \exp(\delta V \times e/kT)$, giving an estimate for K_d(0 mV), with standard error, using SigmaPlot version 8 (Systat Software, Inc., San Jose, CA). δ is the apparent valence, e the elementary charge, k the Boltzmann constant, and T the temperature in kelvin. The fractional residual current (F_{res}), the residual current through a single toxin-bound channel, was analyzed via comparison of single-channel current amplitudes from the unbound and toxin-bound channel (*20*). For whole-cell analysis, toxin k_{on}, k_{off}, and K_d values were adjusted to take into account the F_{res} analysis determined from the bilayer experiments when required. Given the relatively slow binding and unbinding kinetics, the K_d values from the whole-cell experiments should be considered to approximate the values attained following equilibration at the holding potential (see figure legends). Statistical results are reported as means ± the standard error of the mean (SEM) (n), unless otherwise stated.

RESULTS

Comparison of Functional Residues in μCTX PIIIA and μCTX GIIIA. μCTX PIIIA is composed of 22 amino acids with a sequence very similar (64% identical) to that of μCTX GIIIA (Figure 1), in terms of both the size and the spatial arrangement of basic residues (*13*). Each toxin contains an amidated C-terminus and a conserved disulfide framework (1−4, 2−5, 3−6), as well as post-translational amino acid modifications. Hydroxyprolines are found in both μCTX PIIIA and GIIIA, while an N-terminal pyroglutamate residue occurs in only μCTX PIIIA. Both μCTX PIIIA and GIIIA are highly basic peptides, with PIIIA and GIIIA having nominal net charges of +6 and +5, respectively. We examined the effects of different amino acid substitutions in the structure of μCTX PIIIA to determine how

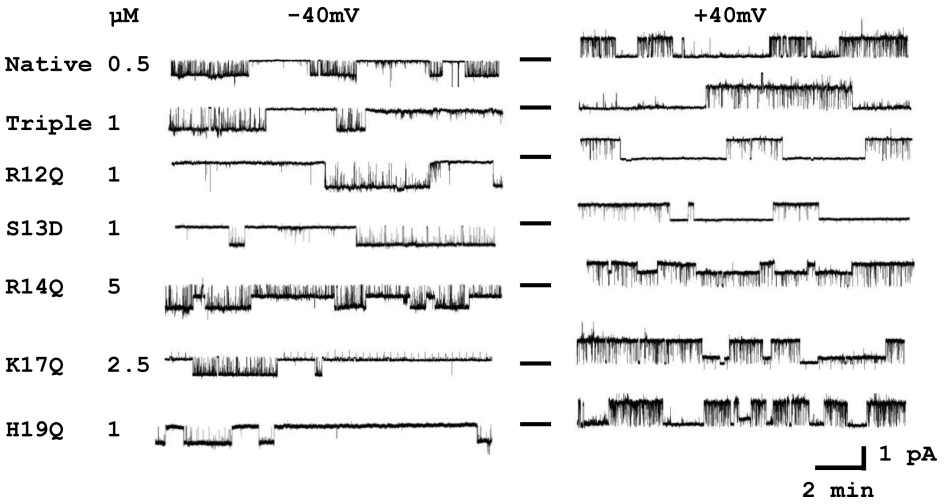

FIGURE 2: Single-channel, steady-state current records from rat skeletal muscle sodium channels in the presence of native μCTX PIIIA, the triple mutant, and representative derivatives with a charge-changing mutation at each position studied. Horizontal bars between each pair of traces represent the baseline nonconducting level (0 pA, closed or blocked). The numerous, brief fluctuations to this level represent intrinsic channel-gating closures. The long (seconds to minutes), low or zero conductance periods represent partial or complete blocking events, respectively. Traces are shown at both 40 and −40 mV; the duration of each trace was 10 min.

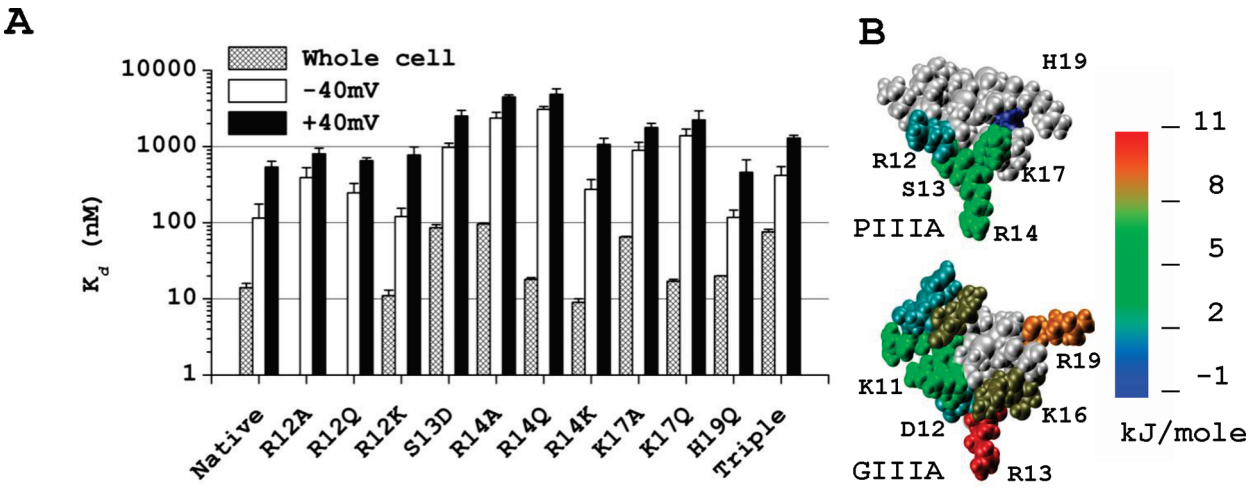

FIGURE 3: Apparent dissociation constants of all μCTX PIIIA derivatives, and changes, $\Delta\Delta G$, in binding energy, which resulted from single-residue substitutions, mapped onto the surfaces of μCTX PIIIA and GIIIA for comparison. (A) Calculated dissociation constants from steady-state bilayer experiments (−40 mV, empty bars; 40 mV, filled bars) and whole-cell experiments (hatched bars; test pulse to −10 mV from a holding potential of −100 mV). (B) $\Delta\Delta G$ values calculated for single-charge changes at each position (R12, S13, R14, K17, and H19 for PIIIA) relative to the native residue mapped onto the surface of both μCTX PIIIA and GIIIA.

individual residues affect toxin binding and the conductance through single, toxin-bound sodium channels. We used 10 single substitutions spread over the surface of the toxin (Figure 1A), and a triple amino acid replacement (PIIIA R12K/S13D/H19Q). Individual substitutions were based on residues previously determined to be important in μCTX GIIIA binding (*25*, *26*), as well as systematic substitutions of the basic residues near the critical R14 (Figure 1B).

For Figures 2−4, most data were obtained from single-channel recordings from rat skeletal muscle channels ($rNa_v1.4$) incorporated into planar lipid bilayers. Such data are compared with results from the whole-cell voltage clamp of cloned $rNa_v1.4$ in Figure 3. In the final section of the Results, we will compare the action of μCTX PIIIA and some selected derivatives on cloned skeletal muscle ($rNa_v1.4$) and neuronal ($rNa_v1.2$) channels expressed in mammalian cells (HEK 293).

Affinity of μCTX PIIIA Derivatives. Figure 2 shows representative steady-state bilayer recordings of currents, through single channels from rat skeletal muscle, in the presence of different μCTX PIIIA derivatives. Traces for each derivative demonstrate that toxin binding was enhanced at the more negative voltage (−40 mV). Some derivatives, e.g., R14Q, show a clear residual current when the peptide was bound (to be further discussed later). Native μCTX PIIIA, S13D, H19Q, and the triple mutant all show complete, all-or-none block of single-channel current. The amplitudes of the full, or partially blocked, unitary current are visible as the envelope of faster, intrinsic channel gating fluctuations, which continue in the presence of the bound toxin (*27*).

Apparent dissociation constants (K_d) determined from steady-state, single-channel bilayer recordings, and from whole-cell patch clamp recordings, are summarized in Figure 3. Whole-cell values represent the higher affinities associated with lower-ionic strength solutions used in those experiments, as previously analyzed in detail (*28*). All of the derivatives tested block single-channel current through $Na_v1.4$. Figure 3A shows that

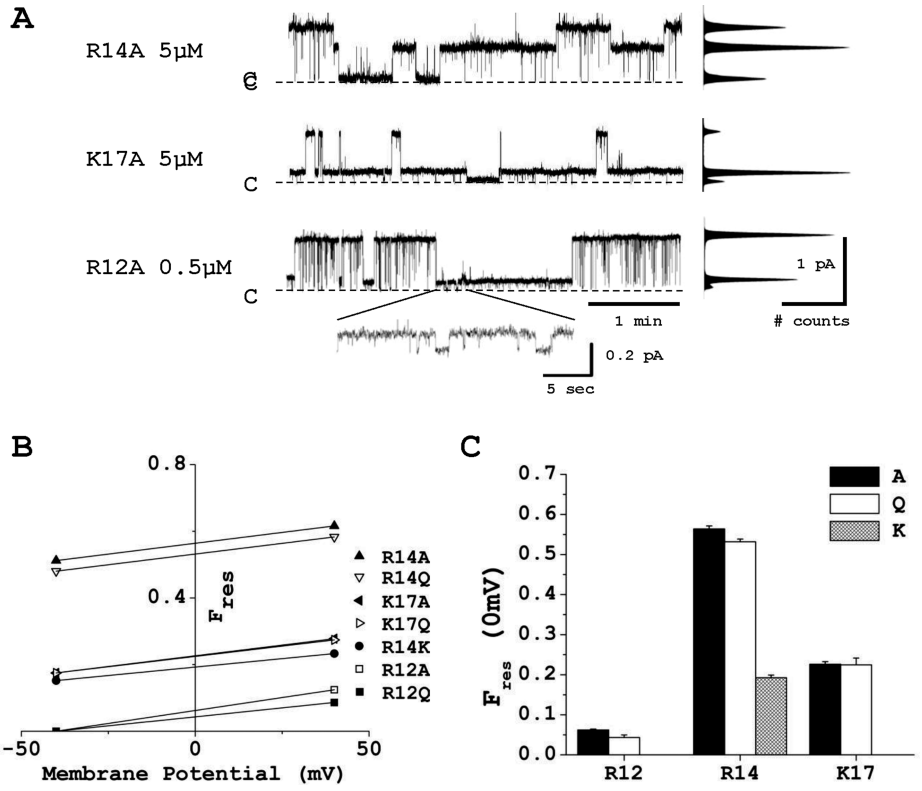

FIGURE 4: Residual single-channel current measurements for μCTX PIIIA derivatives. (A) Individual traces showing the residual current through a single channel, when bound by a PIIIA derivative with alanine substituted for R12, R14, or K17. All-points histograms are shown to the right of each trace. (B) Residual current values at 40 and −40 mV for all R12, R14, and K17 derivatives. (C) F_{res} (0 mV) values determined by interpolation as in panel B for all R12, R14, and K17 derivatives.

the K_d values vary over an approximately 16-fold range, as follows: H19Q < native < R12A < R12Q < R12K < R14K < triple mutant < K17A < S13D < K17A < K17Q < R14A < R14Q.

Native PIIIA exhibited a K_d(0 mV) of 249 ± 161 nM (8). The H19Q substitution, which was intended to make μCTX PIIIA more like μCTX GIIIA by removal of the histidine partial charge at this position, gave a K_d(0 mV) of 232 ± 179 nM (8), a value not significantly different from that of native μCTX PIIIA. All other derivatives of μCTX PIIIA studied show an increase in K_d(0 mV). The R12 mutations show the next smallest changes in affinity, with similar increases in K_d(0 mV) to values of 560 ± 156 (4), 305 ± 250 (5), and 401 ± 63 nM (4) for R12A, R12K, and R12Q, respectively. Mutations at S13, R14, and K17 all gave K_d(0 mV) values in the micromolar range, with S13D, another mutation to make μCTX PIIIA more like GIIIA, giving a K_d(0 mV) of 1.57 ± 0.40 μM. The K17 mutations gave K_d(0 mV) values of 1.26 ± 0.19 (4) and 1.76 ± 0.33 μM (3) for K17A and K17Q, respectively. The largest changes in affinity resulted from charge neutralization at the R14 position, which gave K_d(0 mV) values of 3.25 ± 0.31 (4) and 3.86 ± 0.57 μM (3) for R14A and R14Q, respectively. The charge-conserving substitution, R14K, gave a K_d(0 mV) of 541 ± 279 nM (4), which is closer to that of native μCTX PIIIA than values observed for both of the charge-neutralizing mutations at this position.

The final derivative incorporated three substitutions: R12K, S13D, and H19Q. This was intended to simultaneously mutate three potentially important residues back to the homologous residues found in μCTX GIIIA, in an attempt to recover toxin binding and selectivity close to that of wild-type GIIIA. The K_d(0 mV) of the triple mutant was 710 ± 251 nM (4), more than double that of the native μCTX PIIIA toxin. However, as seen in the last section of Results, the triple mutant discriminates much more strongly between the skeletal muscle and neuronal channels than does wild-type PIIIA.

We calculated ΔΔ*G* values from the changes in K_d(0 mV), which were observed following single-residue substitutions in μCTX PIIIA, and compared them to analogous ΔΔ*G* values calculated for μCTX GIIIA (*26*). In Figure 3B, these are mapped onto the surface of each toxin, with blue showing the smallest ΔΔ*G* values and red the largest change. This mapping immediately highlights the weakened impact of individual residue substitutions in PIIIA compared with GIIIA, especially for substitutions of key Arg and Lys residues.

Incomplete Block Associated with Charge Neutralization at Positions R12, R14, and K17. Single-channel records of block by μCTX PIIIA derivatives with charge-neutralizing substitutions of R12, R14, and K17 and the charge-conserving substitution, R14K, all clearly show a fractional residual current (F_{res}) through peptide-bound single channels. Example traces of residual current from R12A, R14A, and K17A are shown in Figure 4A. The residual current was largest for the R14 derivatives, smaller for the K17 derivatives, and smallest for the R12 derivatives, for which no residual could be detected at −40 mV (Figure 4B). The slight rectification in F_{res} is similar to that reported previously for partially blocking GIIIA derivatives (see ref *20*). For quantitative comparison, values were interpolated to 0 mV. At 0 mV, values of F_{res} were 0.55 ± 0.01 and 0.53 ± 0.01 for R14A and R14Q, respectively, while the charge-conserving substitution, R14K, gave a value of 0.19 ± 0.01 (Figure 4C). The K17 derivatives show F_{res} values of 0.23 ± 0.01 and 0.22 ± 0.02 for the A and Q mutations, respectively. The F_{res} values for R12A and R12Q are 0.06 ± 0.002 and 0.04 ± 0.01, respectively.

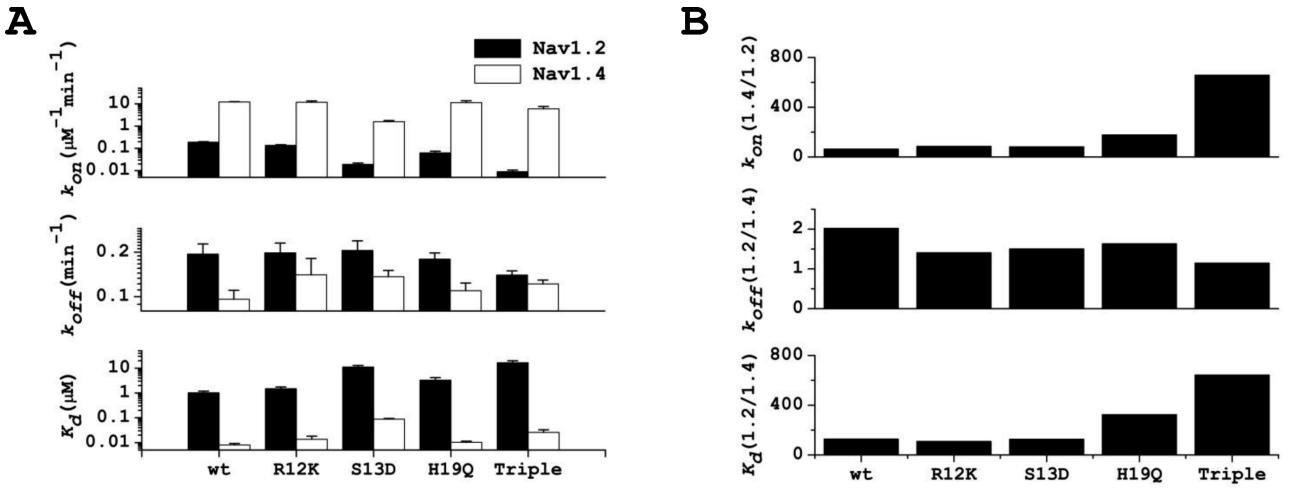

FIGURE 5: Kinetic basis of PIIIA selectivity between skeletal ($Na_v1.4$) and neuronal ($Na_v1.2$) channels. (A) k_{on}, k_{off}, and K_d values for PIIIA, R12K, S13D, H19Q, and the triple mutant (R12K/S13D/H19Q) in $Na_v1.2$ and $Na_v1.4$. (B) Comparison of the k_{on}, k_{off}, and K_d values in $Na_v1.2$ and $Na_v1.4$. Note that the selectivity of PIIIA derivatives for $Na_v1.4$ over $Na_v1.2$ is strongly influenced by differences in the association rate constant, which varies by more than ~3 orders of magnitude for different toxin−channel pairs. In contrast, dissociation rate constants vary only over ~1 order of magnitude (note the logarithmic ordinate scales). The holding potential was −80 mV, with a 2 s prepulse to −140 mV, prior to the test pulse to −10 mV. These data are from a set of experiments different from the set of whole-cell experiments in Figure 3.

The fact that neutralization of a single charge, at any one of three different locations, permits a residual current to pass by the bound peptide represents a striking difference from earlier studies with GIIIA.

Binding and Unbinding Kinetics for μCTX PIIIA Derivatives Reveal a Basis for Discrimination between $Na_v1.2$ and $Na_v1.4$. μCTX PIIIA, the triple mutant, and derivatives containing each individual mutant of the triple mutant were examined using whole-cell patch clamp to determine k_{on}, k_{off}, and K_d (Figure 5A). There were no significant differences among the off rates of the five tested toxins for either $Na_v1.2$ or $Na_v1.4$. However, the off rates were consistently faster in $Na_v1.2$ than in $Na_v1.4$, overall yielding lower affinities, i.e., higher K_d values, for $Na_v1.2$.

The on rates, in both $Na_v1.2$ and $Na_v1.4$, for wild-type PIIIA (0.19 ± 0.01 and 12.0 ± 0.4 μM^{-1} min^{-1}, respectively) were similar to those of the R12K derivative (0.14 ± 0.01 and 11.7 ± 1.7 μM^{-1} min^{-1}, respectively). For $Na_v1.4$, the H19Q derivative showed an on rate (11.2 ± 2.3 μM^{-1} min^{-1}) similar to that of both wild-type PIIIA and the R12K derivative, but its on rate for $Na_v1.2$ (0.06 ± 0.01 μM^{-1} min^{-1}) was lower (~3-fold). The S13D derivative produced a lower on rate, compared to that of wild-type PIIIA, for both $Na_v1.2$ and $Na_v1.4$ (0.019 ± 0.003 and 1.6 ± 0.18 μM^{-1} min^{-1}, respectively). The triple mutant had a slightly lower on rate than wild-type PIIIA for $Na_v1.4$ (5.94 ± 1.64 μM^{-1} min^{-1}), but for $Na_v1.2$, its on rate was dramatically lower (0.009 ± 0.002 μM^{-1} min^{-1}) than that of wild-type PIIIA.

The Triple Mutant Enhances PIIIA's Selectivity for $Na_v1.4$ over $Na_v1.2$. Wild-type PIIIA shows a dissociation constant of 0.008 ± 0.001 μM for $Na_v1.4$; the value is 128-fold higher for $Na_v1.2$ (1.0 ± 0.16 μM), but the triple mutant shows a 624-fold increase in K_d(0 mV) when tested against these two channels (0.03 ± 0.01 and 16.6 ± 3.3 μM, respectively). To determine the contribution of each change in the triple mutant, we tested the three individual substitutions. R12K had K_d values similar to that of wild-type PIIIA for both $Na_v1.2$ and $Na_v1.4$ (1.5 ± 0.3 and 0.013 ± 0.005 μM, respectively), giving a 109-fold difference. The S13D mutant had larger K_d values in both $Na_v1.2$ and $Na_v1.4$ (11.1 ± 1.7 and 0.09 ± 0.005 μM, respectively), but the selectivity for $Na_v1.4$ over $Na_v1.2$ (126-fold) was similar to that of wild-type PIIIA. The H19Q derivative had a K_d value for $Na_v1.4$ of 0.010 ± 0.001 μM, similar to that of wild-type PIIIA. However, for $Na_v1.2$, the dissociation constant was much higher for H19Q (3.30 ± 0.85 μM), yielding a 324-fold selectivity for $Na_v1.4$ over $Na_v1.2$, almost 3 times that seen for wild-type PIIIA. Thus, H19 appears to make the most striking individual contribution to PIIIA's ability to bind to and inhibit $Na_v1.2$. Plots of the ratios of the K_d values and the rate constants (Figure 5B) nonetheless show that the summed effects of R12, S13, and H19 lead to an even more dramatic discrimination between the skeletal and neuronal channels.

DISCUSSION

Precise Targeting versus Broader Actions in μCTX PIIIA and GIIIA. Despite the high degree of sequence identity between PIIIA and GIIIA, and the fact that they both preferentially target $Na_v1.4$, PIIIA does show a modest affinity for neuronal Na_v channels. Native PIIIA has weaker overall binding interactions with $Na_v1.4$ than GIIIA; the apparent K_d(0 mV) equals 36 nM (*26*), versus 249 nM for PIIIA. PIIIA shows cross reactivity with neuronal channels (*13*), while μCTX GIIIA is highly specific for skeletal muscle channels (*7*). The stronger binding interactions between skeletal muscle channels and GIIIA suggest that, in enabling a significant PIIIA affinity for neuronal channels, certain interactions important for highest-affinity binding to skeletal muscle channels are sacrificed. Nonetheless, one would expect a similar binding orientation based on substantial similarities in both sequence and three-dimensional structure.

With GIIIA, a simulated docking constrained by coupling energies from mutant cycle analysis suggests that the key arginine is deep in the vestibule, though somewhat off-axis in the pore lumen (*29*). A new experimental analysis, with additional simulations, each suggests a similar orientation for PIIIA (see ref *30* and a paper in preparation). The ability of a subset of binding orientations to maintain a general docking orientation is also suggested by the results of Hui et al. (*20*). The complex data set shows a striking self-consistency over numerous derivatives, most of which involve double substitutions in the toxin, and is

consistent with a maintained toxin orientation in the face of diverse substitutions.

μCTX PIIIA Derivatives Designed To Emulate the Actions of GIIIA. Recently, μCTXs have been intensely studied because of their striking discrimination among closely related Na_v channel isoforms. Modulators of Na_v channel activity that interact with specific channel isoforms offer a variety of therapeutic possibilities to control pathologic electrical activity in different tissues. An effective way to define the basis of such specificity is to use point mutations in conjunction with assays of the inhibitory activity.

Three individual substitutions in PIIIA were chosen to incorporate the homologous individual residues found in GIIIA. These were R12K, S13D, and H19Q. A triple mutant incorporated all three of these substitutions simultaneously. The insertion of a negatively charged aspartate, in place of S13, yields a decrease in toxin affinity, raising the possibility that a negative charge so close to the critical residue, R14, may destabilize its interactions with the channel. The S13D and R14Q substitutions result in derivatives with similar affinities. This was interesting in that D12, in GIIIA, which is adjacent to the critical R13, seems to have little influence on the efficacy of block. The D12N mutant of GIIIA has an affinity (apparent K_d at 0 mV of 36 nM) only slightly lower than that of the wild-type toxin (50 nM), despite the loss of the aspartate negative charge (*26*).

In PIIIA, the H19Q mutation would remove a partial positive charge from the toxin at pH 7.0. This mutation did not significantly change the K_d(0 mV) for $Na_v1.4$ compared to that of the native toxin (Figure 3). This seems surprising, given the overall dependence of binding of μCTXs on their positively charged residues. The PIIIA triple mutant (R12K/S13D/H19Q), which includes three individual residue replacements to make it more like GIIIA, showed a slight decrease in toxin K_d(0 mV) for $Na_v1.4$ compared with native PIIIA, bringing it closer to the affinity of wild-type GIIIA.

R14 in PIIIA Is a Weaker Determinant of Binding Affinity Than R13 in GIIIA. All μCTXs studied to date have a positively charged arginine or lysine critical to the binding affinity of the toxin. In PIIIA, this residue is R14, which is homologous to R13 in GIIIA and K7 in μCTX KIIIA. The position of the charge, with respect to the backbone carbon, largely determines toxin affinity (*31*, *32*). Tests in different laboratories and on different preparations have shown, for GIIIA, an 80−600-fold increase in the dissociation constant for the R13Q or R13A substitution, while homologous changes in PIIIA yield a smaller increase of ∼10−13-fold. Thus, the overall dominance of this important residue, R14, is reduced in μCTX PIIIA, compared to that in its counterpart μCTX GIIIA (Figure 3B), and is associated with PIIIA's ability to bind to neuronal channels as well as to skeletal muscle channels.

Requirement of R14 in PIIIA for All-Or-None Block. A further illustration of the importance of R14 is that its replacement leads to incomplete block of the channel by the toxin. When the arginine was neutralized to either an alanine or a glutamine, the fractional residual single-channel current level (F_{res}) was 0.55 or 0.53, respectively. These residuals were larger than values seen using μCTX GIIIA [$F_{res} \approx 0.2-0.4$ (*20*, *26*)]. Even though R14 in PIIIA makes a smaller contribution to toxin affinity, its neutral replacement yields a larger residual current than a similar replacement of R13 in GIIIA. This suggests that, similar to R13 in GIIIA, the arginine lies in the permeation pathway and electrostatically and/or sterically occludes current flow (*20*). When R14 was substituted with a charge-conserving residue, a lysine, the binding affinity was only slightly decreased (∼2-fold) compared to the native value, but the bound toxin allowed a residual current of 0.19, despite the conservation of the side chain charge. Wild-type μCTX KIIIA, from *C. kinoshitai*, contains a lysine (K7) at the position homologous to R14 in PIIIA and allows a fractional residual current of ∼0.05−0.17 in $rNa_v1.4$ (unpublished data), similar to that of the PIIIA derivative, R14K. This suggests that the length of the side chain attached to the cationic group in lysine and arginine, and/or the absence of certain N-terminal residues in the shorter KIIIA (compared to GIIIA and PIIIA), could play a role in determining the amplitude of the residual single-channel current.

Neutral Substitutions of R12 and K17 in PIIIA Also Allow Residual Single-Channel Current. Charge-neutralizing substitutions of R12, in PIIIA, with alanine or glutamine, increase the dissociation constant by only ∼1−2-fold, while neutralization mutants at K17 showed larger increases (4−6-fold), closer to that of the R14 replacements. Unlike GIIIA, for which the only single-amino acid mutations that produced residual current were substitutions of R13, we have found three positions in PIIIA at which neutral substitutions allowed residual currents: R12, R14, and K17 (Figure 4). The residual current, $F_{res}(0)$, was largest for R14 (∼0.54) mutations, followed by K17 (∼0.23) and then R12 (∼0.05). The results suggest that these three residues interact with channel residues along the ion permeation pathway and either sterically or electrostatically occlude the pore. KIIIA, a μ-conotoxin, whose native form is highly selective for neuronal channels (*32*), exhibits a similar pattern of residues regulating completeness of block. Thus, the lack of dependence on a single critical residue, such as R13 in GIIIA, is associated with and likely favors the targeting of neuronal as well as skeletal muscle channels by PIIIA (*18*).

The H19Q Substitution and the Triple Mutant Increase μCTX PIIIA's Selectivity for $Na_v1.4$ over $Na_v1.2$. PIIIA is most potent as a blocker of skeletal muscle channels ($Na_v1.4$) but also blocks neuronal channels, exemplified by $Na_v1.2$, with lower affinity. On the other hand, GIIIA is very highly specific for skeletal muscle channels ($Na_v1.4$). In an attempt to explain their different selectivities, we designed a PIIIA triple mutant derivative (R12K/S13D/H19Q) to make PIIIA more like GIIIA. The triple mutant showed a 6-fold stronger selectivity for $Na_v1.4$ over $Na_v1.2$ than did wild-type PIIIA (Figure 5B, ratio of K_d values). To identify contributions of individual residues to the different isoform selectivities, we tested the individual derivatives, R12K, S13D, and H19Q, and found that only H19Q showed a change in selectivity (3-fold increase in affinity for $Na_v1.4$ over $Na_v1.2$, when compared to that of wild-type PIIIA). pH titration of His19 could reveal a pH dependence of the selectivity, but this may be difficult to distinguish from effects mediated by other titratable residues (cf. ref *33*). The observed changes in affinity and selectivity resulted predominantly from changes in k_{on} for binding to $Na_v1.2$ and $Na_v1.4$, as there were only small differences in k_{off} between the two channel isoforms. This contrasts with the results of previous studies of charybdotoxin, a pore blocker of voltage-gated potassium channels. For charybdotoxin, the importance of the kinetic influences is reversed, in that larger changes in affinity resulted from changes in the off rate than changes in the on rate (*34*, *35*). Our discovery, that mutation of the histidine at position 19 increases the selectivity of the toxins for $Na_v1.4$ over $Na_v1.2$, suggests that this histidine contributes to μCTX PIIIA's ability to bind neuronal channels. Notably, a

histidine is found in a similar position in all μCTXs, which block neuronal channels.

CONCLUSIONS

The residual current data, along with the decrease in the overall importance of the pivotal R14 residue as a determinant of binding affinity, show that μCTX PIIIA lacks a critical single residue for all-or-none block. Instead, three residues were each individually required for complete block of the channel. This relationship fits well the simulated docking described in ref *29*, where the arginine side chain did not lie in the center of the pore but was tilted off axis, putting R14 and K17 almost equally close to the narrow selectivity filter of the channel. Compared with that of GIIIA, the flexibility of PIIIA's targeting is associated with its decreased dependence on a single, critical charged residue and the introduction of a histidine at position 19, which is conserved in all μCTXs currently known to target neuronal channels, and appears to underlie the observed changes in selectivity between $Na_v1.2$ and $Na_v1.4$.

SUPPORTING INFORMATION AVAILABLE

Mass spectrometry results and HPLC retention times for μCTX PIIIA and its derivatives. This material is available free of charge via the Internet at http://pubs.acs.org.

REFERENCES

1. Hodgkin, A. L., and Huxley, A. F. (1952) A quantitative description of membrane current and its application to conduction and excitation in nerve. *J. Physiol. 117*, 500–544.
2. Catterall, W. A., Goldin, A. L., and Waxman, S. G. (2005) International Union of Pharmacology. XLVII. Nomenclature and structure-function relationships of voltage-gated sodium channels. *Pharmacol. Rev. 57*, 397–409.
3. George, A. L., Jr. (2005) Inherited disorders of voltage-gated sodium channels. *J. Clin. Invest 115*, 1990–1999.
4. French, R. J., and Terlau, H. (2004) Sodium channel toxins: Receptor targeting and therapeutic potential. *Curr. Med. Chem. 11*, 3053–3064.
5. Spence, I., Gillessen, D., Gregson, R. P., and Quinn, R. J. (1977) Characterization of the neurotoxic constituents of *Conus geographus* (L) venom. *Life Sci. 21*, 1759–1769.
6. Olivera, B. M., and Cruz, L. J. (2001) Conotoxins, in retrospect. *Toxicon 39*, 7–14.
7. Cruz, L. J., Gray, W. R., Olivera, B. M., Zeikus, R. D., Kerr, L., Yoshikami, D., and Moczydlowski, E. (1985) *Conus geographus* toxins that discriminate between neuronal and muscle sodium channels. *J. Biol. Chem. 260* (16), 9280–9288.
8. Terlau, H., and Olivera, B. M. (2004) *Conus* venoms: A rich source of novel ion channel-targeted peptides. *Physiol. Rev. 84*, 41–68.
9. West, P. J., Bulaj, G., Garrett, J. E., Olivera, B. M., and Yoshikami, D. (2002) μ-Conotoxin SmIIIA, a potent inhibitor of tetrodotoxin-resistant sodium channels in amphibian sympathetic and sensory neurons. *Biochemistry 41*, 15388–15393.
10. Bulaj, G., West, P. J., Garrett, J. E., Marsh, M., Zhang, M. M., Norton, R. S., Smith, B. J., Yoshikami, D., and Olivera, B. M. (2005) Novel conotoxins from *Conus striatus* and *Conus kinoshitai* selectively block TTX-resistant sodium channels. *Biochemistry 44*, 7259–7265.
11. Zhang, M. M., Fiedler, B., Green, B. R., Catlin, P., Watkins, M., Garrett, J. E., Smith, B. J., Yoshikami, D., Olivera, B. M., and Bulaj, G. (2006) Structural and functional diversities among μ-conotoxins targeting TTX-resistant sodium channels. *Biochemistry 45*, 3723–3732.
12. Lewis, R. J., Schroeder, C. I., Ekberg, J., Nielsen, K. J., Loughnan, M., Thomas, L., Adams, D. A., Drinkwater, R., Adams, D. J., and Alewood, P. F. (2007) Isolation and structure-activity of μ-conotoxin TIIIA, a potent inhibitor of tetrodotoxin-sensitive voltage-gated sodium channels. *Mol. Pharmacol. 71*, 676–685.
13. Shon, K.-J., Olivera, B. M., Watkins, M., Jacobsen, R. B., Gray, W. R., Floresca, C. Z., Cruz, L. J., Hillyard, D. R., Brink, A., Terlau, H., and Yoshikami, D. (1998) μ-Conotoxin PIIIA, a new peptide for discriminating among tetrodotoxin-sensitive Na channel subtypes. *J. Neurosci. 18* (12), 4473–4481.
14. Al-Sabi, A., McArthur, J., Ostroumov, V., and French, R. J. (2006) Marine toxins that target voltage-gated sodium channels. *Mar. Drugs 4*, 157–192.
15. Shon, K.-J., Grilley, M. M., Marsh, M., Yoshikami, D., Hall, A. R., Kurz, B., Gray, W. R., Imperial, J. S., Hillyard, D. R., and Olivera, B. M. (1995) Purification, characterization, synthesis, and cloning of the lockjaw peptide from *Conus purpurascens* venom. *Biochemistry 34*, 4913–4918.
16. Terlau, H., Shon, K.-J., Grilley, M., Stocker, M., Stühmer, W., and Olivera, B. M. (1996) Strategy for rapid immobilization of prey by a fish-hunting marine snail. *Nature 381*, 148–151.
17. Nielsen, K. J., Watson, M., Adams, D. J., Hammarstrom, A. K., Gage, P. W., Hill, J. M., Craik, D. J., Thomas, L., Adams, D., Alewood, P. F., and Lewis, R. J. (2002) Solution structure of μ-conotoxin PIIIA, a preferential inhibitor of persistent tetrodotoxin-sensitive sodium channels. *J. Biol. Chem. 277*, 27247–27255.
18. Safo, P., Rosenbaum, T., Shcherbatko, A., Choi, D. Y., Han, E., Toledo-Aral, J. J., Olivera, B. M., Brehm, P., and Mandel, G. (2000) Distinction among neuronal subtypes of voltage-activated sodium channels by μ-conotoxin PIIIA. *J. Neurosci. 20*, 76–80.
19. Guo, X., Uehara, A., Ravindran, A., Bryant, S. H., Hall, S., and Moczydlowski, E. (1987) Kinetic basis of the insensitivity to tetrodotoxin and saxitoxin in sodium channels of canine heart and denervated rat skeletal muscle. *Biochemistry 26*, 7546–7556.
20. Hui, K., Lipkind, G., Fozzard, H. A., and French, R. J. (2002) Electrostatic and steric contributions to block of the skeletal muscle sodium channel by μ-conotoxin. *J. Gen. Physiol. 119*, 45–54.
21. Wonderlin, W. F., Finkel, A., and French, R. J. (1990) Optimizing planar bilayer recordings for high resolution with rapid voltage steps. *Biophys. J. 58*, 289–297.
22. Hamill, O. P., Marty, A., Neher, E., Sakmann, B., and Sigworth, F. J. (1981) Improved patch-clamp techniqued for high-resolution current recording from cells and cell-free membrane patches. *Pfluegers Arch. 391*, 85–100.
23. Linford, N. J., Cantrell, A. R., Qu, Y., Scheuer, T., and Catterall, W. A. (1998) Interaction of batrachotoxin with the local anesthetic receptor site in transmembrane segment IVS6 of the voltage-gated sodium channel. *Proc. Natl. Acad. Sci. U.S.A. 95*, 13947–13952.
24. Trimmer, J. S., Cooperman, S. S., Tomiko, S., Zhou, J., Crean, S. M., Boyle, M. B., Kallen, R. G., Sheng, Z., Barchi, R. L., Sigworth, F. J., Goodman, R. H., Agnew, W. S., and Mandel, G. (1989) Primary structure and functional expression of a mammalian skeletal muscle sodium channel. *Neuron 3*, 33–49.
25. Sato, K., Ishida, Y., Wakamatsu, K., Kato, R., Honda, H., Nakamura, H., Ohya, M., Kohda, D., Inagaki, F., Lancelin, J.-M., and Ohizumi, Y. (1991) Active site of μ-conotoxin GIIIA, a peptide blocker of muscle sodium channels. *J. Biol. Chem. 266* (26), 16989–16991.
26. Becker, S., Prusak-Sochaczewski, E., Zamponi, G., Beck-Sickinger, A. G., Gordon, R. D., and French, R. J. (1992) Action of derivatives of μ-conotoxin GIIIA on sodium channels. Single amino acid substitutions in the toxin separately affect association and dissociation rates. *Biochemistry 31* (35), 8229–8238.
27. French, R. J., Prusak-Sochaczewski, E., Zamponi, G. W., Becker, S., Kularatna, A. S., and Horn, R. (1996) Interactions between a pore-blocking peptide and the voltage sensor of the sodium channel: An electrostatic approach to channel geometry. *Neuron 16*, 407–413.
28. Li, R. A., Hui, K., French, R. J., Sato, K., Henrikson, C. A., Tomaselli, G. F., and Marbán, E. (2003) Dependence of μ-conotoxin block of sodium channels on ionic strength but not the permeating $[Na^+]$: Implications for the distinctive mechanistic interactions between Na^+ and K^+ channel pore-blocking toxins and their molecular targets. *J. Biol. Chem. 278*, 30912–30919.
29. Choudhary, G., Aliste, M. P., Tieleman, D. P., French, R. J., and Dudley, S. C., Jr. (2007) Docking of μ-conotoxin GIIIA in the sodium channel outer vestibule. *Channels 1*, 344–352.
30. McArthur, J. R., and French, R. J. (2007) An attempt to determine the orientation of μ-conotoxin binding to sodium channels by mapping the contributions of individual residues to the voltage dependence of block. *Biophys. J. 92* (Suppl.), 178a.
31. Nakamura, M., Niwa, Y., Ishida, Y., Kohno, T., Sato, K., Oba, Y., and Nakamura, H. (2001) Modification of Arg-13 of μ-conotoxin GIIIA with piperidinyl-Arg analogs and their relation to the inhibition of sodium channels. *FEBS Lett. 503*, 107–110.
32. Zhang, M. M., Green, B. R., Catlin, P., Fiedler, B., Azam, L., Chadwick, A., Terlau, H., McArthur, J. R., French, R. J., Gulyas, J., Rivier, J. E., Smith, B. J., Norton, R. S., Olivera, B. M., Yoshikami, D.,

and Bulaj, G. (2007) Structure/function characterization of micro-conotoxin KIIIA, an analgesic, nearly irreversible blocker of mammalian neuronal sodium channels. *J. Biol. Chem. 282*, 30699–30706.
33. Hui, K., McIntyre, D., and French, R. J. (2003) Conotoxins as sensors of local pH and electrostatic potential in the outer vestibule of the sodium channel. *J. Gen. Physiol. 122*, 63–79.
34. Goldstein, S. A. N., Pheasant, D. J., and Miller, C. (1994) The charybdotoxin receptor of a *Shaker* K^+ channel: Peptide and channel residues mediating molecular recognition. *Neuron 12*, 1377–1388.
35. Goldstein, S. A. N., and Miller, C. (1993) Mechanism of charybdotoxin block of a voltage-gated K^+ channel. *Biophys. J. 65*, 1613–1619.
36. Humphrey, W., Dalke, A., and Schulten, K. (1996) VMD: Visual molecular dynamics. *J. Mol. Graphics 14*, 33–38.
37. Berman, H. M., Westbrook, J., Feng, Z., Gilliland, G., Bhat, T. N., Weissig, H., Shindyalov, I. N., and Bourne, P. E. (2000) The Protein Data Bank. *Nucleic Acids Res. 28*, 235–242.